Influence of period-doubling bifurcations in the appearance of border collisions for a ZAD-strategy-controlled buck converter

M. B. D'Amico[1,*,†], F. Angulo[2], G. Olivar[2], E. E. Paolini[1] and J. L. Moiola[1]

[1]*Instituto de Investigaciones en Ingeniería Eléctrica 'Alfredo Desages' (IIIE), Dto. de Ingeniería Eléctrica y de Computadoras, Universidad Nacional del Sur—CONICET Avda Alem 1253, B8000CPB Bahía Blanca, Argentina*
[2]*Department of Electrical and Electronics Engineering and Computer Science, Universidad Nacional de Colombia, Sede Manizales, Cra 27 No. 64–60, Manizales, Colombia*

SUMMARY

The first period-doubling bifurcation of a dc–dc buck converter controlled by a zero-average dynamic strategy is studied in detail. Owing to the saturation of the duty cycle, this bifurcation is followed by a border-collision bifurcation, which is the main mechanism to introduce instability and chaos in the circuit. The multiparameter analysis presented here leads to a complete knowledge of the relatioship between these two bifurcations. The results are obtained by using a frequency-domain approach for the study of period-two oscillations in maps. Copyright © 2010 John Wiley & Sons, Ltd.

1. INTRODUCTION

A dc–dc power converter is an electronic circuit for the purpose of modifying or controlling power from one form to another, generally via a switching action. The basic topologies are known as *buck* and *boost* converters. In a buck converter, the output voltage is smaller than the input voltage. The opposite is true for the boost converter [1, 2].

Power converters are usually modeled by a set of ODEs with discontinuous right-hand side, reflecting the ideal behavior of the electronic switches. Nowadays, most converters are designed to operate periodically under a fixed frequency clock and the control signal (derived from voltage and/or current measures) is the time lapse in which switches are opened or closed during that period. This fixed-frequency PWM behavior makes it possible to find nonlinear maps that describe the current state of the circuit as a function of the state in the previous period [3–5]. It has been widely demonstrated in the literature [6–16] that these nonlinear discrete-time models are more versatile to describe the appearance of different dynamical scenarios (*e.g.* period-doubling bifurcations, Neimark–Sacker bifurcations, discontinuity-induced bifurcations and even chaos) detected in the practice.

A buck converter controlled by a zero-average dynamic (ZAD) strategy is studied in this paper. Fixing the desired output voltage, the control consists basically in obtaining the appropriate duty

*Correspondence to: M. B. D'Amico, Instituto de Investigaciones en Ingeniería Eléctrica 'Alfredo Desages' (IIIE), Dto. de Ingeniería Eléctrica y de Computadoras, Universidad Nacional del Sur—CONICET Avda Alem 1253, B8000CPB Bahía Blanca, Argentina.
†E-mail: mbdamico@uns.edu.ar

cycle of the switches by making zero in average certain surface of the system variables. First proposed in [17], this strategy can be seen as a practical way to implement sliding-mode control since it keeps robustness but operates at a fixed switching frequency. Owing to the inherited discontinuities in their dynamics, the use of sliding-mode laws for controlling dc–dc converters implies the operation at variable switching frequencies, leading to undesirable chattering phenomena. Experimental results comparing the performance of these algorithms can be found in [18, 19].

The dynamical behavior of ZAD-controlled buck converter has been the subject of extensive research [20–25]. It is well known that the operating point of the system becomes unstable and a period-two orbit emerges around it with the variation of a parameter. In [21], it has been shown that this first period-doubling bifurcation is very rapidly followed by a discontinuity-induced bifurcation, known as a border-collision bifurcation, due to the saturation of the duty cycle. This is the main mechanism for introducing chaos, which is observed for further values of the parameter. In [23, 25], it is reported that the variation of an additional parameter leads to a complex bifurcation scenario consisting of period-doubling bifurcations alternating with corner-collision bifurcations. The change in the dynamics of a power converter when two parameters are varied has always received considerable attention [4]. However, the behavior of these circuits is actually defined by more than two parameters.

The aim of this paper is to study the first period-doubling bifurcation exhibited by the ZAD-strategy-controlled buck converter, relating it to the appearance of border-collision bifurcations. In this sense, the variation of four distinguish parameters is considered: namely, a normalized switching period T, a normalized time constant γ, a normalized output voltage reference $x_{1\text{ref}}$ and a control gain k_s. The discrete-time nonlinear model of the converter is studied by using the frequency-domain method for the analysis of period-doubling bifurcations proposed in [26]. By means of an equivalent input–output representation, it is possible to obtain analytical expressions of both the critical bifurcation point and the stability index (noted as σ) of the emerging period-two orbits.

The results presented here enhance the previous contributions [21, 23, 24] derived for specific T and γ values and using state-space methods. Specifically, the analysis not only contemplates variation of more parameters but also considers augmented ranges. Moreover, a physical interpretation (through index σ) of why the birth of period-doubling and border-collision bifurcations can occur on extremely small parameter intervals is given. This detailed information could also help to explain some of the characteristics of the two-parameter bifurcation diagrams exhibited by other dc–dc converters [4].

This paper is organized as follows: In Section 2, the frequency-domain approach for the study of period-doubling bifurcations is briefly reviewed. In Section 3, the ZAD-strategy-controlled dc–dc buck converter and the proposed discrete-time model are described. The analytical expressions obtained by using the frequency-domain approach are included in Section 4. The multiparameter analysis of the bifurcations exhibited by the system is presented in Section 5. Finally, some concluding remarks are given in Section 6.

2. PRELIMINARY CONCEPTS

Traditionally, period-doubling bifurcations in maps are studied by means of the center manifold theorem and the normal form theory [27]. The technique presented in [26] is developed in the frequency-domain employing engineering tools, such as the Nyquist stability criterion, harmonic balance method and Fourier series analysis. The so-called frequency-domain method usually makes it possible to simplify the involved calculations.

The approach is based on the system representation shown in Figure 1, consisting of a closed-loop connection between a $m \times \ell$ linear transfer matrix $\mathbf{G}(\cdot)$ and a smooth (C^r with $r \geqslant 3$) nonlinear function $\mathbf{f}: \mathbf{R}^m \to \mathbf{R}^\ell$. In the figure, $\boldsymbol{\mu} \in \mathbf{R}^s$ is the parameter vector, z is the complex variable of the z-transform, $\mathbf{v}_k \in \mathbf{R}^\ell$ is the input (assumed to be $\mathbf{0}$) and $\mathbf{y}_k \in \mathbf{R}^m$ is the output. The fixed points $\widehat{\mathbf{y}}$ of
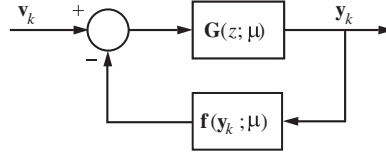
Figure 1. Block diagram of a input–output discrete-time system.

this representation are obtained by solving $\widehat{\mathbf{y}} = -\mathbf{G}(1; \boldsymbol{\mu})\mathbf{f}(\widehat{\mathbf{y}}; \boldsymbol{\mu})$ and the dynamical behavior around $\widehat{\mathbf{y}}$ is studied via the linearized system $\mathbf{G}(z; \boldsymbol{\mu})\mathbf{J}(\boldsymbol{\mu})$ where $\mathbf{J}(\boldsymbol{\mu}) = D_{\mathbf{y}} f(\widehat{\mathbf{y}}; \boldsymbol{\mu})$.[‡]

It is well known that the necessary condition for the existence of period-two oscillations in a state-space map is that one of its eigenvalues crosses the point (-1) in the unit circle for $\boldsymbol{\mu} = \boldsymbol{\mu}_o$. In a input–output representation, this is equivalent to the requirement that the Nyquist diagram of one eigenvalue of matrix $\mathbf{G}(z; \boldsymbol{\mu})\mathbf{J}(\boldsymbol{\mu})$, denoted as $\widehat{\lambda}(z; \boldsymbol{\mu})$, crosses the critical point $(-1+i0)$ for $\boldsymbol{\mu} = \boldsymbol{\mu}_0$ and $z = -1$. Based on [26], if this condition is verified, the procedure for the characterization of the oscillations consists of:

(A) Calculate the right and left eigenvectors associated with $\widehat{\lambda}(-1; \boldsymbol{\mu})$,

$$\mathbf{u}^{\mathrm{T}}\mathbf{G}(-1; \boldsymbol{\mu})\mathbf{J}(\boldsymbol{\mu}) = \mathbf{u}^{\mathrm{T}}\widehat{\lambda}(-1; \boldsymbol{\mu}),$$

$$\mathbf{G}(-1; \boldsymbol{\mu})\mathbf{J}(\boldsymbol{\mu})\mathbf{v} = \widehat{\lambda}(-1; \boldsymbol{\mu})\mathbf{v}.$$

(B) Evaluate matrix $\mathbf{H}(1; \boldsymbol{\mu}) = [\mathbf{I} + \mathbf{G}(1; \boldsymbol{\mu})\mathbf{J}(\boldsymbol{\mu})]^{-1}\mathbf{G}(1; \boldsymbol{\mu})$.
(C) Build matrices $\mathbf{Q} = \{q_{ij}\}$ and $\mathbf{L} = \{l_{ij}\}$ as

$$q_{ij} = \sum_{p=1}^{m} D^2_{y_p y_j} f_i(\widehat{\mathbf{y}}; \boldsymbol{\mu})v_p,$$

$$l_{ij} = \sum_{p=1}^{m} \sum_{q=1}^{m} D^3_{y_p y_q y_j} f_i(\widehat{\mathbf{y}}; \boldsymbol{\mu})v_p v_q,$$

where $i = 1, \ldots, \ell, j = 1, \ldots, m$ and $v_p, v_q, f_i(\cdot)$ are the components of $\mathbf{v}$ and $\mathbf{f}(\cdot)$, respectively.
(D) Find vectors $\mathbf{v}_0 = -\mathbf{H}(1; \boldsymbol{\mu})\mathbf{Q}\mathbf{v}/2$ and $\mathbf{p}(\boldsymbol{\mu}) = \mathbf{Q}\mathbf{v}_0 + \mathbf{L}\mathbf{v}/6$.
(E) Obtain $\xi(\boldsymbol{\mu}) = -\mathbf{u}^{\mathrm{T}}\mathbf{G}(-1; \boldsymbol{\mu})\mathbf{p}(\boldsymbol{\mu})/(\mathbf{u}^{\mathrm{T}}\mathbf{v})$.
(F) Find $\theta_R \in \mathbf{R}$ from $\widehat{\lambda}(-1; \boldsymbol{\mu}) = -1 + \xi(\boldsymbol{\mu})\theta_R^2$ for $\boldsymbol{\mu}_R \neq \boldsymbol{\mu}_0$. If the solution exists, go to Step G; otherwise, end the procedure.
(G) Calculate $\mathbf{Y}_0 = \theta_R^2 \mathbf{v}_0$, $\mathbf{Y}_1 = \theta_R \mathbf{v}$, and approximate the orbit as $\mathbf{y}_k = \widehat{\mathbf{y}} + \mathbf{Y}_0 + \mathbf{Y}_1 e^{\pi i k}$.
(H) Evaluate the stability index

$$\sigma = -\frac{\mathbf{u}^{\mathrm{T}}\mathbf{G}(-1; \boldsymbol{\mu}_0)\mathbf{p}(\boldsymbol{\mu}_0)}{\mathbf{u}^{\mathrm{T}} D_z \mathbf{G}(-1; \boldsymbol{\mu}_0)\mathbf{J}(\boldsymbol{\mu}_0)\mathbf{v}}. \tag{1}$$

(I) If $\sigma > 0 (\sigma < 0)$, the period-two orbit is stable (unstable) and the bifurcation is said to be supercritical (subcritical). However, if $\sigma = 0$, the bifurcation degenerates and the global behavior will be more complex [28].

A map $\mathbf{x}_{k+1} = \mathbf{A}\mathbf{x}_k + \mathbf{B}\mathbf{g}(\mathbf{x}_k; \boldsymbol{\mu})$ with $\mathbf{x}_k \in \mathbf{R}^n$, $\mathbf{A} \in \mathbf{R}^{n \times n}$ (which may be $\mathbf{0}$), $\mathbf{B} \in \mathbf{R}^{n \times \ell}$ and $\mathbf{g}: \mathbf{R}^m \times \mathbf{R}^s \rightarrow \mathbf{R}^\ell$ can always be transformed in a system of the form of Figure 1 by choosing $\mathbf{G}(z; \boldsymbol{\mu}) = \mathbf{C}[z\mathbf{I} - (\mathbf{A} + \mathbf{B}\mathbf{D}\mathbf{C})]^{-1}\mathbf{B}$ and $\mathbf{f}(\mathbf{y}_k; \boldsymbol{\mu}) = \mathbf{D}\mathbf{y}_k - \mathbf{g}(\mathbf{y}_k; \boldsymbol{\mu})$ where $\mathbf{y}_k = \mathbf{C}\mathbf{x}_k$ and $\mathbf{C} \in \mathbf{R}^{m \times n}$, $\mathbf{D} \in \mathbf{R}^{\ell \times m}$ are arbitrary. The representation is not unique and with the proper selection of $\mathbf{C}$ and $\mathbf{D}$,

---

[‡]For the sake of simplicity, $D_{\mathbf{y}}\mathbf{f}(\widehat{\mathbf{y}}; \cdot)_{ij} = \{\partial f_i(\mathbf{y}; \cdot)/\partial y_j\}|_{\mathbf{y} = \widehat{\mathbf{y}}}$ with $\mathbf{f}(\cdot) = [f_1(\cdot) \ldots f_\ell(\cdot)]^{\mathrm{T}}$ and $\mathbf{y} = [y_1 \ldots y_m]^{\mathrm{T}}$; similar expressions will be used for higher-order derivatives.
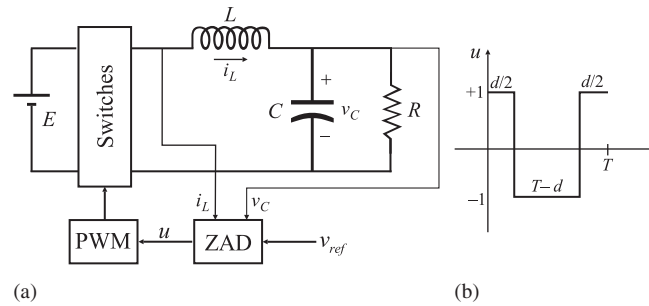
Figure 2. (a) Circuit diagram of a PWM-controlled buck converter and (b) scheme of a centered PWM: the control u is equal to $+1$ the first and last $d/2$ time units, and -1 in the central part of the period.

the dimensions m and ℓ can generally be made smaller than n, leading to more compact results whose derivation could be cumbersome in the time-domain setting.

3. ZAD-STRATEGY-CONTROLLED DC–DC BUCK CONVERTER

The simplified diagram of the buck converter under study is depicted in Figure 2(a). The switches supply the LC low-pass filter with voltages $+E$ and $-E$ during intervals of time governed by a fixed-frequency PWM. The signal v_{ref} corresponds to the required output voltage on the load R. Since only the regulation problem will be analyzed, v_{ref} is considered as a parameter.

Using the normalized variables $x_1 = v_c/E$, $x_2 = i_L E^{-1}\sqrt{L/C}$, $t = \tau/\sqrt{LC}$ and introducing parameters $\gamma = R^{-1}\sqrt{L/C}$, $x_{1\mathrm{ref}} = v_{\mathrm{ref}}/E$ and $T = T_c/\sqrt{LC}$ (where T_c stands for the switching period), the state-space equations of the converter are given by

$$\dot{\mathbf{x}} = \mathscr{A}\mathbf{x} + \mathscr{B}u \tag{2}$$

with

$$\mathscr{A} = \begin{bmatrix} -\gamma & 1 \\ -1 & 0 \end{bmatrix}, \quad \mathscr{B} = \begin{bmatrix} 0 \\ 1 \end{bmatrix}.$$

Since the switches are operated by a centered PWM (see Figure 2(b)), signal u is defined as

$$u = \begin{cases} +1 & \text{if } kT \leqslant t \leqslant kT + d/2, \\ -1 & \text{if } kT + d/2 < t \leqslant kT + (T - d/2), \\ +1 & \text{if } kT + (T - d/2) < t \leqslant kT + T. \end{cases} \tag{3}$$

where ratio $d/T (0 \leqslant d \leqslant T)$, known as duty cycle, is the control variable used to make the output x_1 equal to the reference $x_{1\mathrm{ref}}$.

The ZAD-strategy used here to derive the switching time of the control signal u was first proposed in [17] and studied in more detail in [20]. It can be considered as a modified version of sliding mode control. Given a dynamical system $\dot{\mathbf{x}} = \mathbf{f}(\mathbf{x})$ and a switching surface $s(\mathbf{x}) = 0$, sliding-mode control is based on making the trajectories evolve on $s(\mathbf{x}) = 0$. Thus, $s(\mathbf{x}) = 0$ is fulfilled while the system is on the sliding surface. In a ZAD-strategy, however, $s(\mathbf{x}) = 0$ is fulfilled only in average.[§] Mathematically, $E_T(s(\mathbf{x})) = 0$, where

$$E_T(s(\mathbf{x})) = \frac{1}{T} \int_0^T s(\mathbf{x}(t)) \, \mathrm{d}t. \tag{4}$$

[§]The ZAD-strategy can be seen as a weak version of sliding-mode. Certainly, if $s(\mathbf{x}) = 0$ then $E_T(s(\mathbf{x})) = 0$ but not conversely.

Ideal sliding-mode is not directly implemented in discontinuous systems since it can result in an infinite frequency operation. The ZAD-strategy responds to a practical way of using sliding-mode control where the switching frequency is fixed *a priori* through parameter T.

Surface $s(\mathbf{x})$ is considered here as in [29–31], i.e.

$$s(\mathbf{x}) = (x_1 - x_{1\text{ref}}) + k_s(\dot{x}_1 - \dot{x}_{1\text{ref}}) \tag{5}$$

where k_s is the time constant associated with the first-order dynamics on the surface $s(\mathbf{x})=0$. The calculation of (4) with $s(\mathbf{x})$ defined as (5) in each switching period involves the treatment of a transcendental equation. The dynamical scenario obtained by using the analytical solution of (4)–(5) is presented in [25]. Since it can be extremely complicated to implement such an expression in the practice, it is preferable to consider a piecewise-linear approximation of the error surface, as explained in [18, 20]. Hence, the duty cycle is computed in terms of the system states as $d[kT]/T$ where

$$d[kT] = \frac{T}{2} - \frac{\alpha_1 x_1[kT] - x_{1\text{ref}} + \alpha_2 x_2[kT]}{k_s} \tag{6}$$

with

$$\alpha_1 = 1 - k_s\gamma + \frac{T}{2}(k_s\gamma^2 - \gamma - k_s), \quad \alpha_2 = k_s + \frac{T}{2}(1 - k_s\gamma)$$

and $x_1[kT]$ and $x_2[kT]$ as the state values at the beginning of each cycle [21]. Finally, taking into account that $d[kT]$ should always belong to the interval $[0, T]$, it will be set $d[kT]=T$ if $d[kT] \geqslant T$ or $d[kT]=0$ if $d[kT] \leqslant 0$.

The aim of this paper is to characterize analytically the period-doubling bifurcations exhibited by the system for different parameter values and under the condition $0 < d[kT] < T$. For that purpose, a nonlinear map modeling the state of the circuit at $t=(k+1)T$ as a function of its state at $t=kT$ will be used. Integrating the linear equations resulting from (2)–(3) over a switching period, applying some matrix properties and noting $\mathbf{x}_{k+1}=\mathbf{x}[(k+1)T]$, $\mathbf{x}_k=\mathbf{x}[kT]$ and $d_k=d[kT]$, the so-called Poincaré map is given by

$$\mathbf{x}_{k+1} = e^{\mathscr{A}T}\mathbf{x}_k + (e^{\mathscr{A}T} - \mathbf{I})\mathscr{A}^{-1}\mathscr{B} - 2e^{\mathscr{A}T/2}(e^{\mathscr{A}(T-d_k)/2} - e^{-\mathscr{A}(T-d_k)/2})\mathscr{A}^{-1}\mathscr{B}. \tag{7}$$

Based on the expression of matrix $\mathscr{A}$ and assuming that $\gamma < 2$, the following results

$$e^{\mathscr{A}x} = \begin{bmatrix} \phi_{12}(x) & \phi_2(x) \\ -\phi_2(x) & \phi_{12+}(x) \end{bmatrix}, \tag{8}$$

$$(e^{\mathscr{A}x} - \mathbf{I})\mathscr{A}^{-1}\mathscr{B} = \begin{bmatrix} 1 - \phi_{12+}(x) \\ \gamma - \gamma\phi_{12+}(x) + \phi_2(x) \end{bmatrix}, \tag{9}$$

where $\phi_{12}(x) = \phi_1(x) - \gamma\phi_2(x)/2$, $\phi_{12+}(x) = \phi_1(x) + \gamma\phi_2(x)/2$, $\phi_1(x) = e^{-1/2\gamma x}\cos(\mu x/2)$, $\phi_2(x) = 2e^{-1/2\gamma x}\sin(\mu x/2)/\mu$ and $\mu = \sqrt{4 - \gamma^2}$.

As the third term of (7) reveals, the variable d_k appears on the argument of the exponential matrices making the theoretical bifurcation analysis significantly difficult. This can be simplified by considering the series expansion

$$e^{\mathscr{A}x} = \mathbf{I} + \sum_{n=1}^{\infty} \frac{1}{n!}\mathscr{A}^n x^n.$$

Thus, the terms in (7) depending on d_k can be rewritten as

$$e^{\mathscr{A}(T-d_k)/2} - e^{-\mathscr{A}(T-d_k)/2} = 2\sum_{n=0}^{\infty} \frac{1}{(2n+1)!}\mathscr{A}^{2n+1}\frac{(T-d_k)^{2n+1}}{2^{2n+1}}. \tag{10}$$

The error in the computation of (10) when using a finite number of terms is analyzed in Appendix A.

Then, substituting (8)–(9) into (7) and considering the terms up to the third order of (10), the proposed map modeling the states of the ZAD-controlled buck converter for each period is given by

$$\begin{bmatrix} x_{k+1}^1 \\ x_{k+1}^2 \end{bmatrix} = \begin{bmatrix} \phi_{12}(T) & \phi_2(T) \\ -\phi_2(T) & \phi_{12+}(T) \end{bmatrix} \begin{bmatrix} x_k^1 \\ x_k^2 \end{bmatrix} + \begin{bmatrix} 1-\phi_{12+}(T) \\ \gamma-\gamma\phi_{12+}(T)+\phi_2(T) \end{bmatrix}$$

$$-2\begin{bmatrix} \phi_2\left(\dfrac{T}{2}\right) \\ \phi_{12+}\left(\dfrac{T}{2}\right) \end{bmatrix}(T-d_k) + \frac{1}{12}\begin{bmatrix} \gamma\phi_{12}\left(\dfrac{T}{2}\right)+\phi_2\left(\dfrac{T}{2}\right) \\ \phi_{12}\left(\dfrac{T}{2}\right) \end{bmatrix}(T-d_k)^3 \qquad (11)$$

$$d_k = \frac{T}{2} - \frac{\alpha_1 x_k^1 - x_{1\mathrm{ref}} + \alpha_2 x_k^2}{k_s}.$$

4. FREQUENCY-DOMAIN FORMULAE

The state-space system (11) can be recast as described in Section 2 choosing

$$\mathbf{A} = \begin{bmatrix} \phi_{12}(T) & \phi_2(T) \\ -\phi_2(T) & \phi_{12+}(T) \end{bmatrix}, \quad \mathbf{B} = \begin{bmatrix} 1 & 0 \\ \gamma & 1 \end{bmatrix},$$

$$\mathbf{C} = \begin{bmatrix} 1 & 0 \\ 0 & 1 \end{bmatrix}, \quad \mathbf{D} = \begin{bmatrix} 0 & 0 \\ 0 & 0 \end{bmatrix},$$

$$\mathbf{g}(\widehat{d_k}) = \begin{bmatrix} 1-\phi_{12+}(T)-2\phi_2\left(\dfrac{T}{2}\right)\widehat{d_k} + \dfrac{1}{12}\left[\gamma\phi_{12}\left(\dfrac{T}{2}\right)+\phi_2\left(\dfrac{T}{2}\right)\right]\widehat{d_k^3} \\ \phi_2(T)-2\phi_{12}\left(\dfrac{T}{2}\right)\widehat{d_k} + \dfrac{1}{12}\left[(1-\gamma^2)\phi_{12}\left(\dfrac{T}{2}\right)-\gamma\phi_2\left(\dfrac{T}{2}\right)\right]\widehat{d_k^3} \end{bmatrix},$$

$$\widehat{d_k} = \frac{T}{2} + \frac{1}{k_s}[\alpha_1 \ \ \alpha_2]\mathbf{y}_k - \frac{x_{1\mathrm{ref}}}{k_s},$$

where $\widehat{d_k} = T - d_k$ and $\mathbf{y}_k = \mathbf{x}_k$. Thus, one of the input–output equivalent representation of the ZAD-controlled buck converter is given by

$$\mathbf{G}(z) = q(z)^{-1}\begin{bmatrix} z-\phi_{12}(T) & \phi_2(T) \\ \gamma z-\gamma\phi_{12}(T)-\phi_2(T) & z-\phi_{12}(T) \end{bmatrix},$$

$$\mathbf{f}(\mathbf{y}_k) = -\mathbf{g}(\mathbf{y}_k),$$

with $q(z) = z^2 - 2\phi_1(T)z + \phi_1(T)^2 + \mu^2\phi_2(T)^2/4$.

As mentioned before, fixed points $\widehat{\mathbf{y}}$ can be obtained by solving the nonlinear equation $\widehat{\mathbf{y}} = -\mathbf{G}(1)\mathbf{f}(\widehat{\mathbf{y}})$. Since it is expected that the control strategy makes the output voltage equal to $x_{1\mathrm{ref}}$, it is directly assumed that $\widehat{\mathbf{y}} = [x_{1\mathrm{ref}} \ \ \gamma x_{1\mathrm{ref}}]^T$. The linearization of $\mathbf{f}(\cdot)$ in a neighborhood of this fixed point is

$$\mathbf{J}(k_s) = \frac{1}{k_s}\begin{bmatrix} J_1 \\ J_2 - \gamma J_1 \end{bmatrix} \cdot [\alpha_1 \ \ \alpha_2]$$

where

$$J_1 = 2\phi_2\left(\frac{T}{2}\right) - \frac{T^2}{16}\left[\phi_2\left(\frac{T}{2}\right) + \gamma\phi_{12}\left(\frac{T}{2}\right)\right](1-x_{1\text{ref}})^2,$$

$$J_2 = 2\left[\phi_{12}\left(\frac{T}{2}\right) + \gamma\phi_2\left(\frac{T}{2}\right)\right] - \frac{T^2}{16}\phi_{12}\left(\frac{T}{2}\right)(1-x_{1\text{ref}})^2.$$

Since $\det[\mathbf{G}(z)\mathbf{J}(k_s)] = 0$, the unique nontrivial eigenvalue of the system is

$$\widehat{\lambda}(z;k_s) = \frac{(\alpha_1 J_1 + \alpha_2 J_2)z - (\alpha_1\phi_{12+}(T) + \alpha_2\phi_2(T))J_1 + (\alpha_1\phi_2(T) - \alpha_2\phi_{12}(T))J_2}{k_s q(z)}.$$

The necessary condition for the existence of a period-doubling bifurcation is $\widehat{\lambda}(-1;k_s) = -1 + \mathrm{i}0$. Solving this equation, the critical value of the gain k_s as a function of the rest of the parameters can be written as

$$k_{\text{sc}} = \frac{g_1(T,\gamma) + g_2(T,\gamma)(1-x_{1\text{ref}})^2}{g_3(T,\gamma) + g_4(T,\gamma)(1-x_{1\text{ref}})^2}. \tag{12}$$

where

$$g_1(T,\gamma) = 8\left\{(1+\phi_1(T))\left(2\phi_2\left(\frac{T}{2}\right) + T\phi_{12}\left(\frac{T}{2}\right)\right)\right.$$
$$\left. + \phi_2(T)\left[(T-\gamma)\phi_2\left(\frac{T}{2}\right) + \frac{1}{2}(T\gamma-4)\phi_{12}\left(\frac{T}{2}\right)\right]\right\},$$

$$g_2(T,\gamma) = \frac{T^2}{4}(1+\phi_1(T))\left[(T\gamma-2)\phi_2\left(\frac{T}{2}\right) + (T\gamma^2-2\gamma-T)\phi_{12}\left(\frac{T}{2}\right)\right]$$
$$+ \frac{T^2}{8}\phi_2(T)\left[(T\gamma^2-2\gamma-2T)\phi_2\left(\frac{T}{2}\right) + (T\gamma^3-2\gamma^2-3T\gamma+4)\phi_{12}\left(\frac{T}{2}\right)\right],$$

$$g_3(T,\gamma) = 8\left\{(1+\phi_1(T))\left[T\phi_2\left(\frac{T}{2}\right) + (T\gamma-2)\phi_{12}\left(\frac{T}{2}\right)\right]\right.$$
$$\left. + \frac{1}{2}\phi_2(T)\left[(T\gamma-4)\phi_2\left(\frac{T}{2}\right) + (T\gamma^2-2\gamma-2T)\phi_{12}\left(\frac{T}{2}\right)\right] + q(-1)\right\},$$

$$g_4(T,\gamma) = \frac{T^2}{4}(1+\phi_1(T))\left[(T\gamma^2-2\gamma-T)\phi_2\left(\frac{T}{2}\right) + (T\gamma^3-2\gamma^2-2T\gamma+2)\phi_{12}\left(\frac{T}{2}\right)\right]$$
$$+ \frac{T^2}{8}\phi_2(T)\left[(T\gamma^3-2\gamma^2-3T\gamma+4)\phi_2\left(\frac{T}{2}\right) + (T\gamma^4-2\gamma^3-4T\gamma^2+6\gamma+2T)\phi_{12}\left(\frac{T}{2}\right)\right].$$

Following steps A–H of Section 2, it is possible to determine the stability of the orbits exhibited by the converter when (12) is verified. The eigenvectors associated to the linearized system (step A) are

$$\mathbf{v} = \begin{bmatrix} v_1 \\ 1 \end{bmatrix} = \begin{bmatrix} \dfrac{(1+\phi_{12+}(T))J_1 - \phi_2(T)J_2}{(1+\phi_{12}(T))J_2 + \phi_2(T)J_1} \\ 1 \end{bmatrix}, \quad \mathbf{u}^{\mathrm{T}} = \begin{bmatrix} \dfrac{\alpha_1}{\alpha_2} & 1 \end{bmatrix}.$$

The closed-loop matrix of Step B is

$$\mathbf{H}(1; k_s) = \frac{1}{r(1)} \begin{bmatrix} k_s q(1) + h_{11} & h_{12} \\ h_{21} & k_s q(1) + h_{22} \end{bmatrix} \mathbf{G}(1),$$

$$h_{11} = (1 - \phi_{12}(T))\alpha_2 J_2 - \phi_2(T)\alpha_2 J_1,$$

$$h_{12} = -(1 - \phi_{12+}(T))\alpha_2 J_1 - \phi_2(T)\alpha_2 J_2,$$

$$h_{21} = -(1 - \phi_{12}(T))\alpha_1 J_2 + \phi_2(T)\alpha_1 J_1,$$

$$h_{22} = (1 - \phi_{12+}(T))\alpha_1 J_1 + \phi_2(T)\alpha_1 J_2,$$

$$r(1) = k_s q(1) + h_{11} + h_{22}.$$

After some algebraic operations, matrices $\mathbf{Q}$ and $\mathbf{L}$ related to the derivatives of the nonlinear function (step C) can be written as

$$\mathbf{Q} = \frac{T(1 - x_{1\mathrm{ref}})(v_1 \alpha_1 + \alpha_2)(\alpha_1 + \alpha_2)}{4k_s^2} \begin{bmatrix} -\phi_{212}\left(\dfrac{T}{2}\right) \\ \gamma\phi_{212}\left(\dfrac{T}{2}\right) - \phi_{12}\left(\dfrac{T}{2}\right) \end{bmatrix},$$

$$\mathbf{L} = \frac{2(v_1 \alpha_1 + \alpha_2)}{k_s T(1 - x_{1\mathrm{ref}})} \mathbf{Q}$$

with $\phi_{212}(x) = \phi_2(x) + \gamma\phi_{12}(x)$. Finally, calculating vectors $\mathbf{v}_0$ and $\mathbf{p}(k_s)$ of step D at the critical point, the stability index σ (step H) is given by

$$\sigma = \frac{(v_1 \alpha_1 + \alpha_2)^2}{96 k_{sc}^2} \frac{\sigma_1 \sigma_2}{\sigma_3} \tag{13}$$

with

$$\sigma_1 = \left[\phi_{212}\left(\frac{T}{2}\right)(2 + \phi_1(T) + \gamma\phi_2(T)) - 2\phi_2(T)\phi_{12}\left(\frac{T}{2}\right)\right]\alpha_1$$

$$+ \left[2\phi_{212}\left(\frac{T}{2}\right)\phi_2(T) + 2(1 + \phi_1(T))\phi_{12}\left(\frac{T}{2}\right) - \gamma\phi_2(T)\phi_{12}\left(\frac{T}{2}\right)\right]\alpha_2$$

$$\sigma_2 = \frac{3T^2}{4}\left(\sigma_1 - 4\phi_{212}\left(\frac{T}{2}\right)\alpha_1 - 4\phi_{12}\left(\frac{T}{2}\right)\alpha_2\right)(1 - x_{1\mathrm{ref}})^2 - 4r(1),$$

$$\sigma_3 = r(1)[J_1 \alpha_1 + J_2 \alpha_2 - 2k_{sc}(1 + \phi_1(T))].$$

5. MULTIPARAMETER ANALYSIS

Based on expressions (12) and (13) derived above, the changes exhibited by the detected period-doubling bifurcations under the variation of $x_{1\mathrm{ref}}$, T and γ are described. The parameter values are restricted according to the following practical and analytical considerations:

(i) $|x_{1\mathrm{ref}}| \leqslant 1$. This range corresponds to the duty cycle limits ($0 \leqslant d_k \leqslant T$).
(ii) $0 < T \leqslant \frac{2}{3}$. The switching frequency (or equivalently, for this case, the sampling frequency) of the converter has to be greater than the cut-off frequency of the filter LC ($f = 1/(2\pi\sqrt{LC})$).
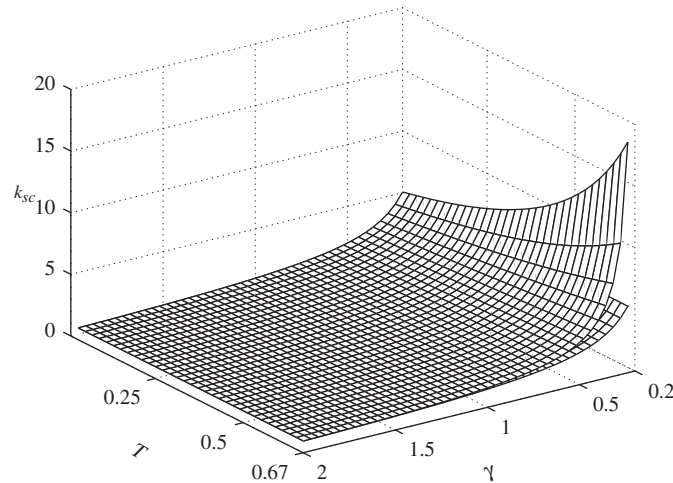
Figure 3. Upper and lower bounds of k_{sc} for $0 < T < \frac{2}{3}$ and $0.2 \leqslant \gamma < 2$.

Even though the theoretical minimum is $2f$, it is very common practice to choose switching frequencies of around $10f$ (i.e. $T_c \approx \pi\sqrt{LC}/5$). For this reason, it is considered that the normalized period is smaller than $\frac{2}{3}$.

(iii) $0.2 \leqslant \gamma < 2$. This interval is due to considerations of the previous section. The lower limit is related to the expression of the equilibrium point. For $\gamma < 0.2$, $\widehat{\mathbf{y}}$ depends strongly on the parameter values, deviating from the assumption $\widehat{\mathbf{y}} = [x_{1\mathrm{ref}} \ \gamma x_{1\mathrm{ref}}]^{\mathrm{T}}$. This difference affects greatly the calculations of the critical gain. Thus, for example, deviations of around 10% from the actual $\widehat{\mathbf{y}}$ can result in differences between (12) and the k_{sc} values obtained numerically of more than 50%. The upper limit is related to the exponential matrices (8–9). For $\gamma \geqslant 2$, the eigenvalues of matrix $\mathscr{A}$ become real and the proposed solution for $e^{\mathscr{A}x}$ is not valid.

Within this parameter region, coefficients of the critical gain (12) satisfy $g_1(T, \gamma) > 0$, $g_2(T, \gamma) < 0$ and $g_3(T, \gamma) > 0$. However, the sign and magnitude of $g_4(T, \gamma)$ in the denominator of (12) depends on the γ values. Nevertheless, it is explained in Appendix B that it is possible to find upper and lower bounds for k_{sc}. They actually correspond to evaluate (12) at $x_{1\mathrm{ref}} = 1$ and $x_{1\mathrm{ref}} = -1$, respectively. Thus,

$$\frac{g_1(T, \gamma) + 4g_2(T, \gamma)}{g_3(T, \gamma) + 4g_4(T, \gamma)} \leqslant k_{\mathrm{sc}} \leqslant \frac{g_1(T, \gamma)}{g_3(T, \gamma)}.$$

The maximum and minimum of k_{sc} as a function of T and γ are shown in Figure 3. As it can be observed, both surfaces approaches asymptotically as γ increases, indicating that the influence of $x_{1\mathrm{ref}}$ over k_{sc} could be neglected when γ is big enough. Figure 4 depicts the critical period-doubling curves obtained by fixing, for instance,[¶] $T = 0.1767$ and considering $\gamma = 0.35$, 0.85, 1.35 and 1.85. In these cases, the variation of k_{sc} for $-1 \leqslant x_{1\mathrm{ref}} \leqslant 1$ decreases[‖] from 13.69% ($\gamma = 0.35$) to 1.85% ($\gamma = 1.85$). These figures also show that the curves move to greater gain values as γ decreases.

The stability of the bifurcations is determined by index (13). For any combination of $x_{1\mathrm{ref}}$, T and γ inside the proposed region, index σ results greater than 0, so that the period-doubling bifurcations exhibited by the system are always supercritical (i.e. period-two oscillations are stable and they appear when the fixed point is unstable). Moreover, the magnitude of σ is usually very close to 0, indicating that oscillations tend to grow suddenly. The bifurcation diagrams given in [20, 21] clearly present this behavior.

[¶]To facilitate the comparisons, the T value is the same used in the references [20, 21, 23].

[‖]Percentages of variation are measured with respect to minimum values, i.e. $100(\max[k_{sc}] - \min[k_{sc}])/\min[k_{sc}]$.
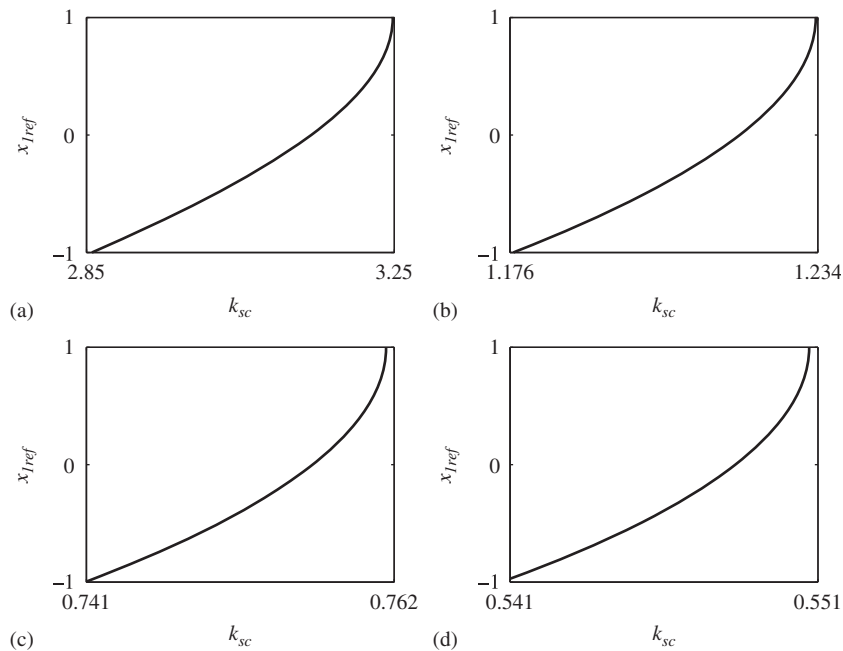
Figure 4. Period-doubling curves for $T=0.1767$ and different γ values: (a) $\gamma=0.35$; (b) $\gamma=0.85$; (c) $\gamma=1.35$; and (d) $\gamma=1.85$.

For an arbitrary pair of (T,γ) values, the influence of $x_{1\text{ref}}$ over the stability of the period-doubling bifurcations can again be neglected. As an example, Figure 5 shows that the variation of σ over the curves of Figure 4 does not exceed the 8.5% in any of the four cases. Thus, bifurcations corresponding to the same critical curve in Figure 4 are almost equal. As it is illustrated in Figure 6 for $T=0.1767$, $\gamma=0.35$ and different $x_{1\text{ref}}$ values, the bifurcation points change slightly and branches grow all in the same way. Hence, the point of the upper branch where d_k achieves T ($d_k/T=1$), i.e. where a border collision appears, is directly related to the level of the reference and not to the growth of the bifurcation. As $x_{1\text{ref}}$ increases, the interval of k_s where the period-doubling bifurcation exists reduces, making the nonsmooth phenomena [20, 23] appear closer to the critical gain k_{sc}.

Changes in the σ values are more visible when now parameters T and γ are varied and $x_{1\text{ref}}$ is fixed, as it is depicted in Figure 7. In particular, σ clearly diminishes when T and γ are close to their upper limits, meaning that the branches of the period-doubling bifurcation grow more abruptly. Figure 8 illustrates this behavior increasing γ from 0.35 to 1.85 for $T=0.1767$ and $x_{1\text{ref}}=0.8$. As it can be seen, the greater the γ value, the faster the growth of the branches (since σ decreases from 0.07799 to 0.06321). This phenomenon actually implies that the point where d_k reaches T ($d_k/T=1$) will depend crucially on the γ value for the same level of reference. In fact, the border collision will be nearer the period-doubling bifurcation point as γ increases (since σ decreases).

It is worth mentioning that simulations concerning border-collision bifurcations have not been presented in this section since this paper is mainly focused on the characteristics of their antecessor. Different scenarios including both period-doubling and border-collisions bifurcations for $T=0.1767$ and $\gamma=0.35$ can be found in [23, 24].

6. CONCLUSIONS

This paper reported detailed analytical and numerical developments in the multiparameter study of the first period-doubling bifurcation of a ZAD-strategy-controlled buck converter. Using a frequency-domain approach, critical values for a relevant parameter k_s as a function of the remaining
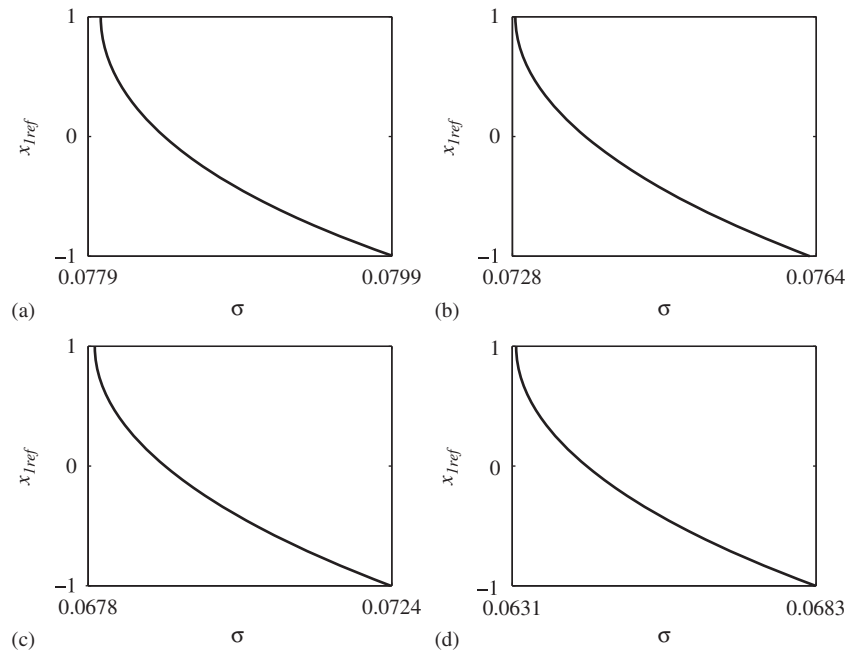
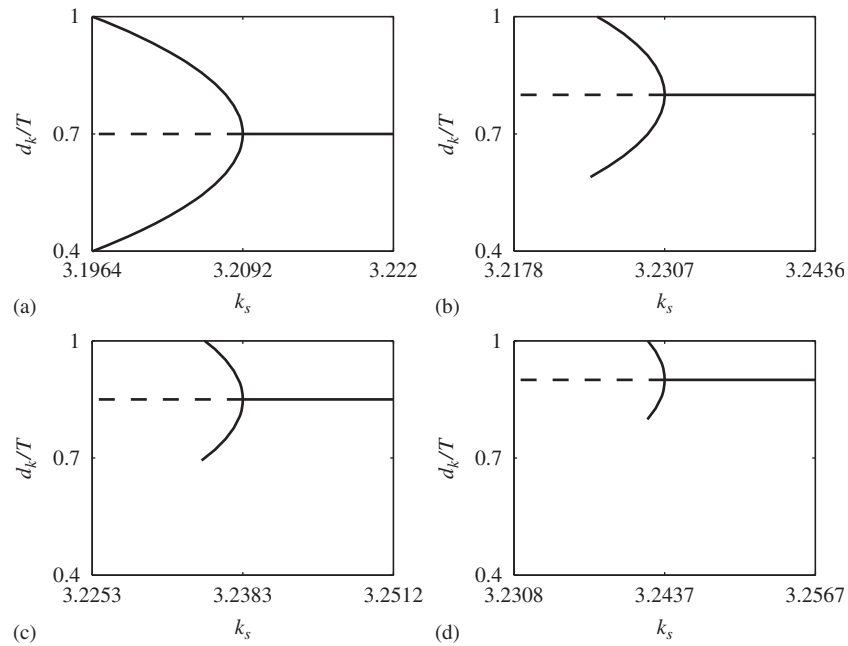Figure 5. Stability index values corresponding to the period-two critical curves of Figure 4.

Figure 6. Period-doubling bifurcations for $T=0.1767$, $\gamma=0.35$ and different $x_{1\mathrm{ref}}$ values. The variation of gain k_s is defined as $k_{sc}\pm 4\%$ in all cases: (a) $x_{1\mathrm{ref}}=0.4$; (b) $x_{1\mathrm{ref}}=0.6$; (c) $x_{1\mathrm{ref}}=0.7$; and (d) $x_{1\mathrm{ref}}=0.8$.

parameters were obtained, and a stability index was computed. It was demonstrated that for an arbitrary pair of T and γ values, the characteristics of the period-doubling bifurcation practically keep unchanged. So, the point where a border collision appears is directly related to the reference $x_{1\mathrm{ref}}$. Changes are visible when T and γ are varied and $x_{1\mathrm{ref}}$ is fixed. In particular, the appearance of a border collision will be nearer the birth of the period-doubling bifurcation as γ increases.
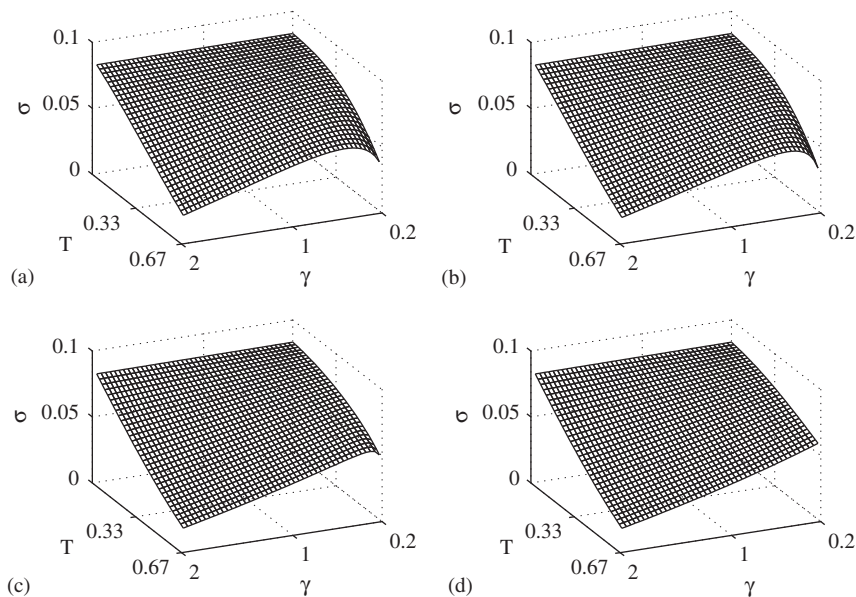
Figure 7. Stability index evaluated at $0<T\leqslant 2/3$, $0.2\leqslant\gamma<2$ and different $x_{1\mathrm{ref}}$ values: (a) $x_{1\mathrm{ref}}=-1$; (b) $x_{1\mathrm{ref}}=-0.5$; (c) $x_{1\mathrm{ref}}=0.5$; and (d) $x_{1\mathrm{ref}}=1$.
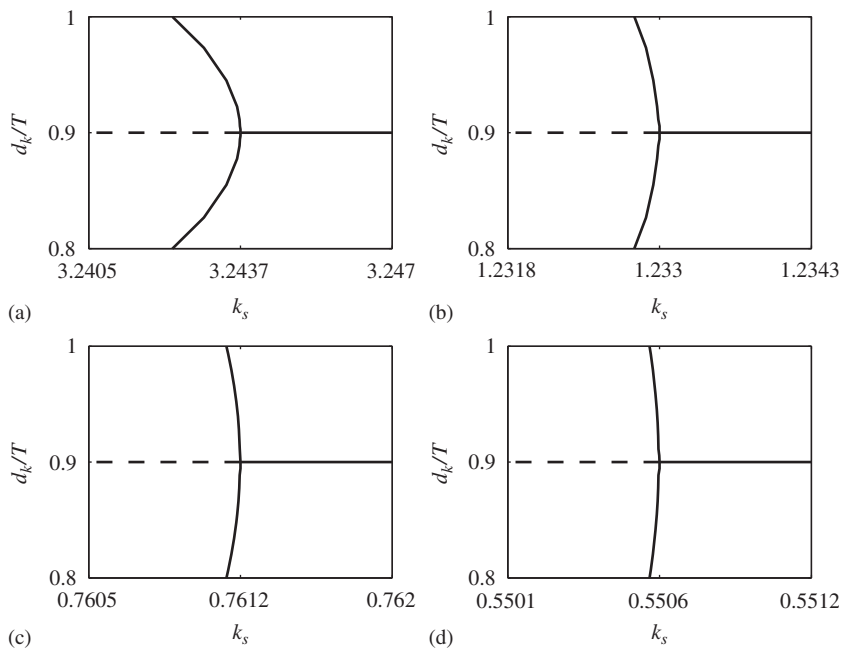

Figure 8. Period-doubling bifurcations for $T=0.1767$, $x_{1\mathrm{ref}}=0.8$ and different γ values. The interval of variation of k_s is $[0.999k_{\mathrm{sc}}, 1.001k_{\mathrm{sc}}]$: (a) $\gamma=0.35$; (b) $\gamma=0.85$; (c) $\gamma=1.35$; and (d) $\gamma=1.85$.

Although the results were strictly restricted to the γ interval where all analytical assumptions are valid, it could be expected they were still correct for a wider range of this parameter.

APPENDIX A

The following reasoning is based on that presented in [5] for the approximation of transition matrix $\mathrm{e}^{\mathscr{A}x}$.

The term in (7) depending on the control variable d_k can be replaced by the infinite series

$$e^{\mathscr{A}(T-d_k)/2} - e^{-\mathscr{A}(T-d_k)/2} = 2\sum_{n=0}^{\infty} \frac{1}{(2n+1)!} \mathscr{A}^{2n+1} \frac{(T-d_k)^{2n+1}}{2^{2n+1}}. \tag{A1}$$

But, assuming that only the first N terms are used, i.e.

$$e^{\mathscr{A}(T-d_k)/2} - e^{-\mathscr{A}(T-d_k)/2} \approx \mathscr{A}(T-d_k) + \cdots + \frac{1}{(2N+1)!} \mathscr{A}^{2N+1} \frac{(T-d_k)^{2N+1}}{2^{2N}}, \tag{A2}$$

the error is given by

$$\varepsilon = \frac{1}{(2N+3)!} \mathscr{A}^{2N+3} \frac{(T-d_k)^{2N+3}}{2^{2(N+1)}} + \frac{1}{(2N+5)!} \mathscr{A}^{2N+5} \frac{(T-d_k)^{2N+5}}{2^{2(N+2)}} + \cdots$$

An upper bound for the elements of matrix ε can be found by using the ∞-norm**. Thus,

$$|\varepsilon_{ij}| \leqslant 2\sum_{n=N+1}^{\infty} \frac{1}{2^{2n+1}(2n+1)!} |(i,j) \text{ element of} (\mathscr{A}(T-d_k))^{2n+1}|$$

$$\leqslant 2\sum_{n=N+1}^{\infty} \frac{1}{2^{2n+1}(2n+1)!} \|\mathscr{A}(T-d_k)\|^{2n+1}$$

$$\leqslant \frac{\|\mathscr{A}(T-d_k)\|^{2N+3}}{2^{2(N+1)}(2N+3)!} \left(1 + \frac{\|\mathscr{A}(T-d_k)\|^2}{2^2} + \frac{\|\mathscr{A}(T-d_k)\|^4}{2^4} + \cdots\right)$$

Considering that $\|\mathscr{A}(T-d_k)\| < 2$, the infinite series in the right side of the inequality converges. Hence, an upper bound ϑ of the error is

$$\vartheta = \frac{\|\mathscr{A}(T-d_k)\|^{2N+3}}{2^{2(N+1)}(2N+3)! \left(1 - \dfrac{\|\mathscr{A}(T-d_k)\|^2}{4}\right)}.$$

For the ZAD-controlled buck converter under study, $\|\mathscr{A}(T-d_k)\| \leqslant (\gamma+1)T$ so that parameter values should verify $T < 2/(\gamma+1)$. Thus, for example, if (A1) is replaced by (A2) with $N=1$, the error for $T = \frac{1}{2}$ and $\gamma = 1$ is $\vartheta \leqslant 6.94 \times 10^{-4}$, meaning that this number of terms represents a reasonably close approximation for the involved matrices. In fact, it can be seen that (A2) with $N=1$ works properly even if $T > 2/(\gamma+1)$.

APPENDIX B

The upper bound for the critical gain k_{sc} is deduced in the following. The lower bound can be found a similar way.

Within the parameter region defined in Section 5, it can be seen that $g_1(T,\gamma) > 0$, $g_2(T,\gamma) < 0$, $g_3(T,\gamma) > 0$ and also $|g_1(T,\gamma)| >> 4|g_2(T,\gamma)|$. Furthermore, $g_1(T,\gamma) + g_2(T,\gamma)(1-x_{1\text{ref}})^2 > 0$ because $(1-x_{1\text{ref}})^2 \leqslant 4$. However, the sign and magnitude of $g_4(T,\gamma)$ in the denominator of (12) depends on the γ values.

If $g_4(T,\gamma) > 0$, it results $g_3(T,\gamma) + g_4(T,\gamma)(1-x_{1\text{ref}})^2 > 0$. Furthermore,

$$0 < 1 + \frac{g_2(T,\gamma)}{g_1(T,\gamma)}(1-x_{1\text{ref}})^2 \leqslant 1 \leqslant 1 + \frac{g_4(T,\gamma)}{g_3(T,\gamma)}(1-x_{1\text{ref}})^2.$$

**The ∞-norm of a matrix A is defined as $\|A\| = \max_i \sum_j |a_{ij}|$. In particular, $|a_{ij}| \leqslant \|A\|$ for all i and j.

Rewriting (12) as

$$k_{sc} = \frac{g_1(T,\gamma)}{g_3(T,\gamma)} \frac{1 + \dfrac{g_2(T,\gamma)}{g_1(T,\gamma)}(1-x_{1\text{ref}})^2}{1 + \dfrac{g_4(T,\gamma)}{g_3(T,\gamma)}(1-x_{1\text{ref}})^2}, \tag{B1}$$

it can be affirmed that

$$k_{sc} \leqslant \frac{g_1(T,\gamma)}{g_3(T,\gamma)}.$$

If $g_4(T,\gamma)<0$, it results again $g_3(T,\gamma)+g_4(T,\gamma)(1-x_{1\text{ref}})^2>0$ since $|g_3(T,\gamma)|>>4|g_4(T,\gamma)|$ and $0\leqslant(1-x_{1\text{ref}})^2\leqslant4$. Moreover, it is obtained that

$$\frac{g_2(T,\gamma)}{g_1(T,\gamma)} < \frac{g_4(T,\gamma)}{g_3(T,\gamma)}.$$

Thus,

$$0 < 1 + \frac{g_2(T,\gamma)}{g_1(T,\gamma)}(1-x_{1\text{ref}})^2 < 1 + \frac{g_4(T,\gamma)}{g_3(T,\gamma)}(1-x_{1\text{ref}})^2,$$

and taken into account (B1), it can be deduced that

$$k_{sc} \leqslant \frac{g_1(T,\gamma)}{g_3(T,\gamma)}.$$

REFERENCES

1. Mohan N, Undeland TM, Robbins WP. *Power Electronics*: *Converters, Applications and Design*. Wiley: New York, 1995.
2. Ang SS, Oliva AR. *Power Switching Converters* (2nd edn). CRC Press: New York, 2005.
3. di Bernardo M, Vasca F. Discrete-time maps for the analysis of bifurcations and chaos in DC/DC converters. *IEEE Transactions on Circuits Systems I* 2000; **47**(2):130–142.
4. Banerjee S, Verghese GC. *Nonlinear Phenomena in Power Electronics*: *Attractors, Bifurcations, Chaos, and Nonlinear Control*. IEEE Press: New York, 2001.
5. Tse CK. *Complex Behavior of Switching Power Converters*. CRC Press: Boca Raton, 2004.
6. Chan WCY, Tse CK. Study of bifurcations in current-programmed DC/DC boost converters: from quasi-periodicity to period-doubling. *IEEE Transactions on Circuits Systems I* 1997; **44**(12):1129–1142.
7. di Bernardo M, Fossas E, Olivar G, Vasca F. Secondary bifurcations and high periodic orbits in voltage controlled buck converter. *International Journal of Bifurcation and Chaos* 1997; **7**:2755–2771.
8. Banerjee S, Chakrabarty K. Nonlinear modelling and bifurcations in the boost converter. *IEEE Transactions on Power Electronics* 1998; **13**(2):252–260.
9. di Bernardo M, Garofalo F, Glielmo L, Vasca F. Switchings, bifurcations and chaos in DC/DC converters. *IEEE Transactions on Circuits Systems I* 1998; **45**(2):133–141.
10. Yuan G, Banerjee S, Ott E, Yorke JA. Border-collision bifurcations in the buck converter. *IEEE Transactions on Circuits Systems I* 1998; **45**(7):707–716.
11. Banerjee S, Grebogi C. Border collision bifurcations in two-dimensional piecewise smooth maps. *Physical Review E* 1999; **59**:4052–4061.

12. El Aroudi A, Benadero L, Toribio E, Olivar G. Hopf bifurcation and chaos from torus breakdown in a PWM voltage-controlled DC-DC boost converter. *IEEE Transactions on Circuits Systems I* 1999; **46**(11):1374–1382.

13. Suto Z, Nagy I. Analysis of nonlinear phenomena and design aspect of three-phase space vector modulated converters. *IEEE Transactions on Circuits Systems I* 2003; **50**(8):1064–1071.

14. Zhusubaliyev ZT, Mosekilde E. *Bifurcations and Chaos in Piecewise-Smooth Dynamical Systems*, vol. 44. World Scientific Co.: Singapore, 2003.

15. El Aroudi A, Debbat M, Giral R, Olivar G, Benadero L, Toribio E. Bifurcations in dc-dc switching converters: Review of methods and applications. *International Journal of Bifurcation and Chaos* 2005; **15**(5):1549–1578.

16. Huang Y, Iu HHC, Tse CK. Boundaries between fast- and slow-scale bifurcations in parallel-connected buck converters. *International Journal of Circuit Theory and Applications* 2008; **36**(5):681–695.

17. Fossas E, Grinó R, Biel D. Quasi-sliding control based on pulse width modulation, zero average and the l_2 norm. In *Advances in Variable Structure System*, *Analysis*, *Integration and Applications*, Yu X, Xu JX (eds). World Scientific Co.: 2001.

18. Biel D, Fossas E, Ramos R, Guinjoan F. Implementación de controles pseudo-sliding en sistemas conmutados (in spanish). *Congreso Latinoamericano de Control Automático*, Guadalajara (Mexico), 2002.

19. Ramos R, Biel D, Fossas E, Guinjoan F. Fixed-frequency quasi-sliding control algorithm: application to power inverters design by means of FPGA implementation. *IEEE Transactions on Power Electronics* 2003; **18**(1): 344–355.

20. Angulo F. Análisis de la dinámica de convertidores electrónicos de potencia usando PWM basado en promediado cero de la dinámica del error (zad), available at http://www.tdx.cesca.es/tdx-0727104-095928 (in spanish). *PhD Thesis*, Universidad Politécnica de Cataluña, Spain 2004.

21. Angulo F, Fossas E, Olivar G. Transition from periodicity to chaos in a PWM-controlled buck converter with ZAD strategy. *International Journal of Bifurcation and Chaos* 2005; **15**(10):3245–3264.

22. Angulo F, Ocampo C, Olivar G, Ramos R. Nonlinear and nonsmooth dynamics in a dc-dc buck converter: two experimental set-ups. *Nonlinear Dynamics* 2006; **46**(3):239–257.

23. Angulo F, Olivar G, di Bernardo M. Two-parameter discontinuity-induced bifurcation curves in a ZAD strategy-controlled DC–DC buck converter. *IEEE Transactions on Circuits Systems I* 2008; **55**(8):2392–2401.

24. Angulo F, Olivar G, Taborda A. Continuation of periodic orbits in a ZAD-strategy controlled buck converter. *Chaos*, *Solitons and Fractals* 2008; **38**(2):348–363.

25. Fossas E, Hogan SJ, Seara TM. Two-parameter bifurcation curves in power electronic converters. *International Journal of Bifurcation and Chaos* 2009; **19**(1):349–357.

26. D'Amico MB, Moiola JL, Paolini EE. A frequency domain method for analyzing period doubling bifurcations in discrete-time systems. *Circuits*, *Systems and Signal Processing* 2004; **23**:516–535.

27. Kuznetsov YA. *Elements of Applied Bifurcation Theory*. Springer: New York, 1995.

28. D'Amico MB, Moiola JL, Paolini EE. Study of degenerate bifurcations in maps: a feedback system approach. *International Journal of Bifurcation and Chaos* 2004; **14**(5):1625–1641.

29. Bilalovic F, Music O, Sabanović A. Buck converter regulator operating in the sliding mode. *VII Power Conversion International Conference*, Geneva, Switzerland, 1983; 331–340.

30. Venkataramanan R, Sabanović A, Ćuk S. Sliding mode control of dc-to-dc converters. *IECON 1985*, San Francisco, U.S.A., 1985; 251–258.

31. Carpita M, Marchesoni M, Oberti M, Puguisi L. Power conditioning system using slide mode control. *IEEE Power Electronics Specialist Conference*, Kyoto, Japan, 1988; 623–633.